ISSN 0947-8396, Volume 101, Number 1

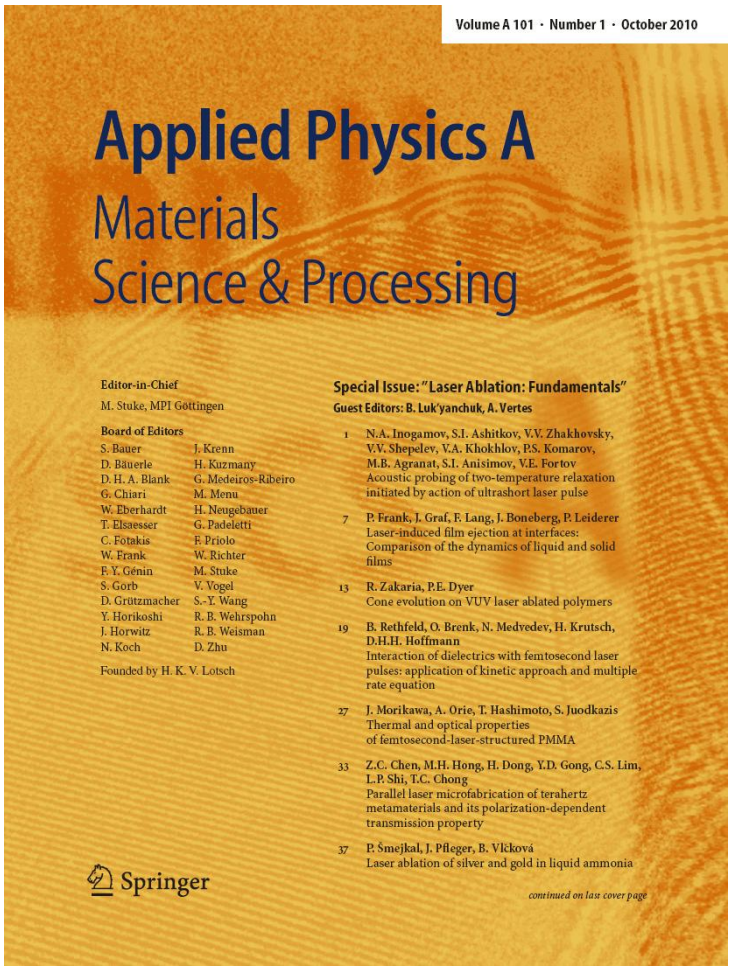

**This article was published in the above mentioned Springer issue.
The material, including all portions thereof, is protected by copyright;
all rights are held exclusively by Springer Science + Business Media.
The material is for personal use only;
commercial use is not permitted.
Unauthorized reproduction, transfer and/or use
may be a violation of criminal as well as civil law.**

Appl Phys A (2010) 101: 1–5
DOI 10.1007/s00339-010-5765-2

Author's personal copy

Applied Physics A
Materials Science & Processing

Acoustic probing of two-temperature relaxation initiated by action of ultrashort laser pulse

N.A. Inogamov · S.I. Ashitkov · V.V. Zhakhovsky · V.V. Shepelev · V.A. Khokhlov · P.S. Komarov · M.B. Agranat · S.I. Anisimov · V.E. Fortov

Received: 6 November 2009 / Accepted: 27 April 2010 / Published online: 28 May 2010
© Springer-Verlag 2010

Abstract Ultrashort laser pulse transfers metal into a two-temperature warm dense matter state and triggers a chain of hydrodynamic and kinetic processes—melting, expansion, stretching, creation of tensile stress and transition into metastable state. We study the response of aluminum film deposited on a glass substrate to irradiation by a pump laser pulse transmitted through glass. Several films with thicknesses from 350 to 1200 nm have been investigated. The smallest thickness is of the order of the heating depth $d_T \sim 100$ nm in Al. The d_T-layer and the free rear side of the film are coupled through pressure waves propagating between them. Therefore, the processes within d_T-layer affects the time dependent displacement $\Delta x_{rear}(t)$ of the rear surface. We compare simulated and experimental dependencies $\Delta x_{rear}(t)$ obtained by the pump–probe technique. It allows us to define a thickness of molten Al layer and explore the two-temperature processes occurring inside the heated layer.

N.A. Inogamov (✉) · V.A. Khokhlov · S.I. Anisimov
Institute for Theoretical Physics, Russian Academy of Sciences, Chernogolovka, 142432, Russia
e-mail: nailinogamov@googlemail.com

S.I. Ashitkov · V.V. Zhakhovsky · P.S. Komarov · M.B. Agranat · V.E. Fortov
Joint Institute of High Temperature, Russian Academy of Sciences, Moscow, 125412, Russia

V.V. Zhakhovsky
Department of Physics, University of South Florida, Tampa, FL 33620, USA

V.V. Shepelev
Institute for Computer Aided Design, Russian Academy of Sciences, Moscow, 123056, Russia

1 Introduction

Ultrashort laser pulse (usLP) transforms a near surface layer into two-temperature warm dense matter (2T-WDM) state with hot electrons and cold crystal lattice (ions): $T_e \gg T_i$, where T_e and T_i are temperatures of electrons and ions. For pulse durations $\tau_L \sim 10$–100 fs and absorbed fluences $F_{abs} \sim 100$ mJ/cm^2, at the time ~ 100 fs from the beginning of the pulse, the penetration depth of the electron thermal wave (EThW) is of the order of the skin depth $\delta_{skin} \sim 10$–20 nm for metals. Deeper heating $d_T \sim (5$–$15)\delta_{skin}$ by the EThW takes place during the time τ_{ei} of the electron–ion (e–i) relaxation to an equilibrium state having $T_e = T_i$ [1–3]. It takes $\tau_{ei} \sim 3$ ps in our conditions.

This is because the electrons, firstly, have the low heat capacity $C_e < C_i$ ($T_e < T_F$), and, secondly, they are weakly thermally coupled with ion subsystem in the 2T-WDM state. Therefore, their heat diffusivity χ_e, and thus the depth $d_T \sim \sqrt{\chi_e \tau_{ei}}$, is significantly higher [4] than the value $\chi \sim 1$ cm^2/s from reference books. The last value corresponds to one-temperature conditions $T_e = T_i$. The EThW moves slowly after finishing of the e–i relaxation ($t > \tau_{ei}$).

The electron energy balance is

$$\rho D_t(E_e/\rho) = (\kappa T_e')' - p_e u' - \alpha (T_e - T_i) + Q, \qquad (1)$$

where $D_t = \partial_t + u\partial_x$, $u' = \partial u/\partial x$, Q is laser energy source. The main factors in (1), which determine d_T, are the coefficient α of e–i energy exchange and the heat conductivity κ, since $\kappa = \chi_e C_e$ and $\tau_{ei} \sim (T_i/T_e)C_i/\alpha$. The estimate for τ_{ei} follows from the lattice energy balance $\rho D_t(E_i/\rho) = -p_i u' + \alpha (T_e - T_i)$, $\Delta E_i \approx C_i \Delta T_i$.

In our conditions F_{abs} is higher than the melting threshold F_m. Because aluminum in the heated layer melts fast [1], the depth d_T may be found from the thickness of the molten

layer, since the last is of the order of d_T. In turn, the depth d_T is determined by the coefficients α and κ in (1). The coefficient $\alpha \approx 3.6 \cdot 10^{17}$ W/K/m^3 [5] is well known for Al. Therefore, the depth d_T can be used to obtain the poorly known 2T thermal conductivity κ. In the work we compare simulations, based on the values κ taken from [4], with results of the pump–probe experiments. Agreement between them may mean that the theory [4] gives the right value for the coefficient $\kappa(T_e, T_i, \rho)$.

Dynamics of the d_T-layer (heating, melting, pressure build-up, expansion) determines formation of acoustic waves and rear-side displacements $\Delta x_{frn}(t)$ and $\Delta x_{rear}(t)$, where $\Delta x_{frn}(t)$ and $\Delta x_{rear}(t)$ are shifts of the frontal glass–Al interface (irradiated by pump pulse) and rear-side boundary of Al film from their initial positions. In the paper the pump–probe interferometry is used to measure the phase ψ and reflectivity R changes at the rear-side boundary relative to their initial values ψ_0, R_0 before action of pump pulse [1, 6]. The ψ data give the shift Δx_{rear} of the rear-side boundary after arrival of pressure wave/perturbation.

2 Acoustics related to supersonic heating

It is well known that usLP triggers thermomechanical phenomena, e.g. see [3, 7], illustrated by Fig. 1 for the case where usLP comes from the left side and the absorbing target is closed by a glass substrate slowing expansion of heated Al. The cold pressure curves of glass SiO_2 and Al are very close [8] in compressed states. Therefore, in linear acoustic approximation the glass–Al boundary weakly reflects acoustic waves passing through the interface. This corresponds to the case with acoustic decay of initially motionless pressure bump into right-moving ("plus") and left-moving ("minus") waves, as shown in Fig. 1. The width of the "plus" wave carries information about the heat penetration depth d_T. The pump–probe technique may pickup this information, when the "plus" wave arrives to the rear-side boundary of a film.

The purpose of this work is to study two new thermomechanical effects besides the well-known effect of formation of pressure bump ant its decomposition on two sonic waves. They are: (a) the imprint of the peculiarity of the Grüneisen coefficient Γ into pressure profile, and (b) formation of the tail of the right-moving wave as result of nonlinearity. The peculiarity of Γ shown in Fig. 2 is a result of melting. The difference between equilibrium and non-equilibrium melting is discussed below. The discussion is based on comparison of equilibrium two-temperatures hydrodynamic (2T-HD) simulation [1] and molecular dynamics (MD) simulation [7] which accounts for non-equilibrium melting. This peculiarity causes premature breaking of the "plus" wave, because between the two markers in Fig. 2 the

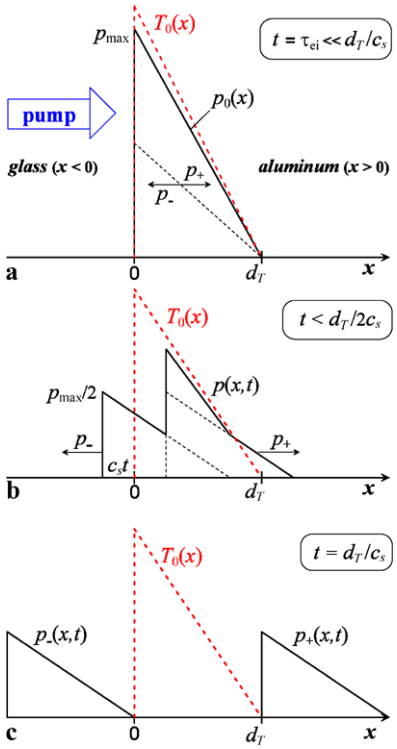

Fig. 1 From top to bottom: (**a**) ultrafast heating of Al by usLP with supersonic increase of temperature, and pressure during τ_{ei}, (**b**, **c**) sonic d'Alembert decay of the pressure bump into two compression waves propagating to the left and to the right sides. The temperature bump remains in its position due to the difference in behavior between sonic and entropy modes of perturbations. Thermal conduction in glass is very small, therefore, the heat from Al does not penetrate into glass

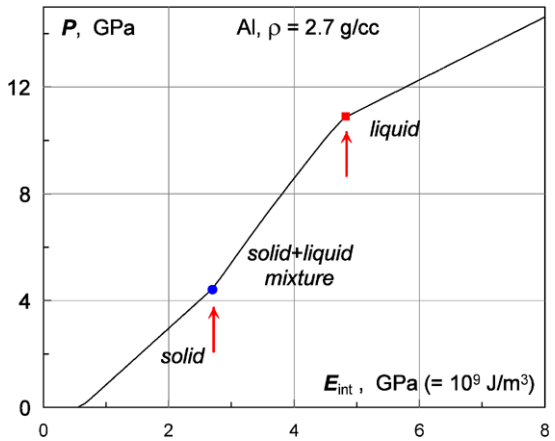

Fig. 2 The kinks at the dependence $p(\rho = \text{const}, E_{int})$ are caused by equilibrium melting. The kinks imprint themselves into hydrodynamic profiles. The thermodynamic dependence $p(\rho, E_{int})$ is taken from the wide-range equation of state [8]

dependence $p(\rho)$ is steeper than in the smooth case without melting.

Wave breaking is a nonlinear effect appearing as a result of dependence of sound speed on amplitude of a prop-

Author's personal copy

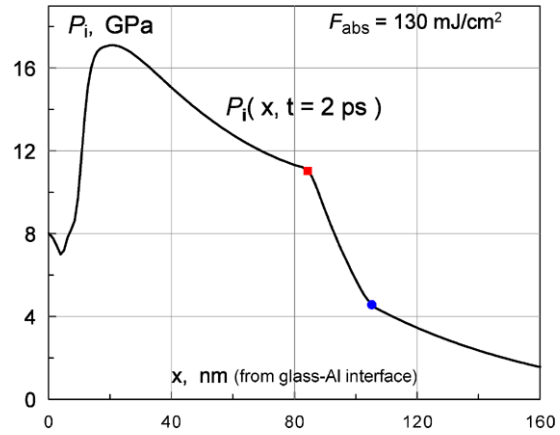

Fig. 3 Ionic pressure profile at the supersonic stage of ion heating by fast EThW. The markers at the profile correspond to the markers in Fig. 2. This is snapshot taken from 2T-HD simulation. The 2T-HD code uses the equation of state [8] shown in previous figure

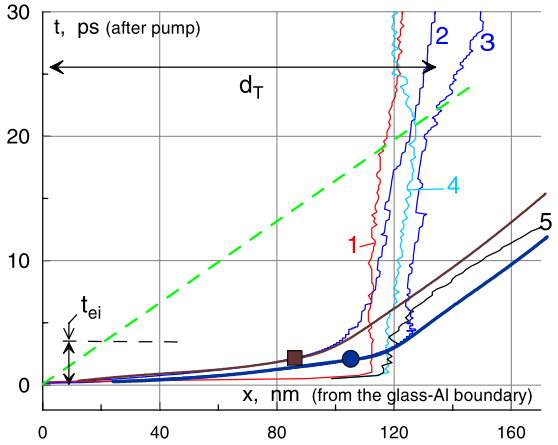

Fig. 4 Radiation of the sonic perturbation by the 2T supersonic EThW when this wave transforms from supersonic $t < \tau_{ei}$ to subsonic $t > \tau_{ei}$ regime. The radiation takes place when the pressure curves (the MD *curve 5* and two 2T-HD curves around) break away from the melting (the *curves 1–3*) and temperature (*curve 4*, MD, $T = 1.3$ kK) fronts. Curve 1 is a melting front trajectory obtained in MD simulation. The curve with the *round* (*square*) marker corresponds to beginning (end) of melting in 2T-HD. *Curve 5* gives the MD isobaric trajectory for $p = 5$ GPa between the markers in Figs. 2 and 3. The acoustic *curve 5* and two curves around carry away to the rear-side boundary the imprint of the fast melting. Pump–probe measuring of this imprint supplies us with information about 2T processes, that implies the acoustic probing

agating wave. Therefore, the high amplitude part of a wave overtakes the lower amplitude part, which is running ahead [9–11]. The maximum slope at the profile increases during this process. This maximum is achieved in the inflection point. When this slope becomes infinitely large—then a shock appears [9–11]. The slope varies smoothly as a function of spatial coordinate at the instantaneous wave profile.

For the case of supersonic melting the smooth passing through the inflection disappears—since there are kinks at the profile; see Fig. 3. The interval of solid-liquid mixture between the markers in Fig. 3 is the most steep. The slope at this interval becomes steeper as time goes on. This interval replaces the point of inflection. Later this interval transforms entirely to a shock. Thus, the amplitude of a shock jump shortly after breaking is larger for the case of fast melting in comparison with gradual growth of this amplitude from zero in the case without melting. It should be emphasized that the breaking takes place in the regime of acoustic propagation – significantly later e–i equilibration.

There is a transition from the first regime of united supersonic propagation of thermal and pressure profiles at $t < \tau_{ei}$ to the second regime of separated motions of a thermal wave and a pressure wave for the time $t > \tau_{ei}$. This supersonic to sonic/subsonic transition is shown in Fig. 4. Sonic/subsonic here means that the sonic (or pressure) wave and the thermal wave in the second regime are sonic and subsonic, resp. In the first regime the electron internal energy E_e (1) transforms to ion subsystem in e–i energy exchange process. This isochorically increases the ionic pressure p_i. The profile in Fig. 3 corresponds to the first regime. The circle and square markers on the pressure and melting curves in Fig. 4 coincide during the united propagation.

In Fig. 4 the 2T regime is confined inside the horizontal stripe τ_{ei}. In this regime the curves 1 (MD example, $F_{abs} = 82$ mJ/cm^2), and two curves with markers (2T-HD examples, $F_{abs} = 130$ mJ/cm^2) have large velocities. The curves follow the melting process. These examples (different codes and F_{abs}) illustrate the sharp transition from supersonic to subsonic regime. The MD curve 1 gives the isosymmetry trajectory of the symmetry index $s = 2.5$ [1]. The index measures the value of the local disorder. The value $s = 2.2$ corresponds to pure (without inclusions of pieces of unmelted lattice) liquid. The value of $\tau_{ei} \sim 1$ ps, during which the Langevin thermostat warms up the d_T-layer, is shorter for the MD curve than it is in the 2T-HD simulation. In Al the duration $\tau_{ei} \sim 3$ ps is quite short, therefore for fixed d_T taken from 2T-HD and used in MD simulation the influence of the value of this duration is small at later stage $t \gg \tau_{ei}$.

In Fig. 4 the dashed line represents the characteristic starting from the glass–Al boundary after arrival of the pump usLP. This characteristic corresponds to the left edge of the plus wave in Fig. 1. The pressure in the melting zone drops after crossing of the melting zone by this characteristic. It results in decrease of the melting temperature $T_m(\rho \approx \rho_{ini}, p)$. Hence, under high pressure the isothermal $T = 1.3$ kK curve 4 is ahead of the melting front 1 shown in Fig. 4, and curve 4 is behind the front 1 after crossing. It means that under high pressure $T_m > 1.3$ kK, while under low pressure $T_m < 1.3$ kK.

The effect (a) of acoustic trace of fast melting has been discussed above. Let us consider now the effect (b) of the nonlinear tail. In linear acoustics the plus wave in Fig. 1

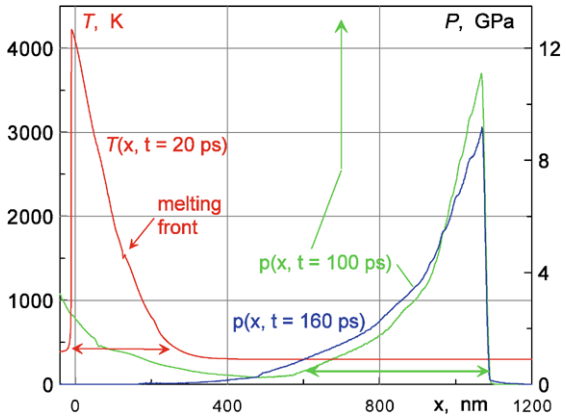

Fig. 5 Extension of the pressure profile due to nonlinear reflection at the glass–Al boundary. The pressure profile is wider than the temperature profile which produces the pressure profile—compare the *horizontal arrows*

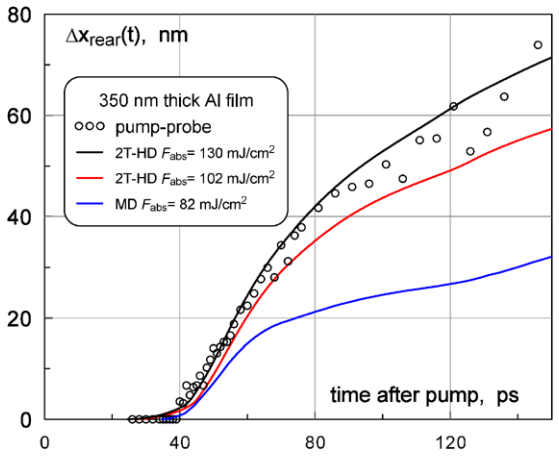

Fig. 6 Transformation of pressure profile into time dependence of the shift Δx_{rear}. The Al film thickness is 350 nm, $\tau_L = 90$ fs, $\tau_{\text{FWHM}} = 150$ fs. The F_{abs} in simulation is adjusted to fit the experimental data

terminates in the characteristic starting from the point $x = 0, t = 0$, that is a dashed line in Fig. 4. In the nonlinear case the significant density difference appears between cold glass and hot Al as a result of expansion (decay of initial jump). It causes reflection from this boundary even if we suppose that initially the glass and Al acoustic impedances are equal. This is a nonlinear effect since reflection depends on the amplitude of heating.

The nonlinear reflection of the minus wave from the glass–Al boundary greatly extends the width of the acoustic wave propagating to the right side. The pump–probe measurements detect this extension. The extended pressure profiles are shown in Fig. 5. The full width of the $p(x, t = 100$ ps) profile is 470 nm, whereas the width of the T-profile is ≈ 270 nm at the time $t = 20$ ps. At this time the characteristic starting from the point $x = 0, t = 0$ crosses the d_{T}-layer; see Fig. 4. The width of the T-profile gives the width of the plus pressure wave (Fig. 1) without the tail. The two widths of the $T(x, t = 20$ ps) and $p(x, t = 100$ ps) profiles are marked by two horizontal arrows in Fig. 5.

The amplitude of the pressure tail relates to the temperature of Al at the glass–Al boundary after e–i relaxation. In its turn, this temperature is linked to the 2T electron heat conductivity κ: since higher κ corresponds to lower temperatures. There is also widening of the acoustic profile $p(x, t)$ as a result of dispersion—the decrease of c_s with decrease of pressure causes divergence of characteristics [9–11]. But this effect is weaker than the extension due to nonlinear reflection. Comparison of two profiles at $t = 100$ and 160 ps is shown in Fig. 5. The profile $t = 100$ ps is shifted to the position of the $p(x, t = 160$ ps) profile. The maximum of the profile $t = 100$ ps before the shift is marked by the vertical arrow. The tail appears as a result of nonlinear interaction of the acoustic mode (that is the minus wave shown in Fig. 1) and the entropy mode (it is shown as the T-profile in Fig. 1). In linear acoustic these modes passes through each other without any trace.

In experiments by [12] the laser beam comes through glass to the Ni film. The rear-side shift $\Delta x_{\text{rear}}(t)$ has been measured. In experimental work [13] the laser beam irradiates Al film from a vacuum side. Only shock velocity has been measured. Fluence and therefore pressures were several times higher and films were thicker than in present work. This shift was measured experimentally for Al film and compared with simulated one in our work. Comparison of calculated and experimental profiles of the shift is shown in Fig. 6.

In summary, we find two new acoustic phenomena caused by thermomechanical response of metal film to usLP irradiation. They are the imprint of 2T supersonic melting into acoustic signal and formation of the pressure tail due to nonlinear interaction of acoustic and entropy modes. We show that the model [4] for 2T κ describes well the experimental data.

Acknowledgement The work has been supported by the RFBR grant No. 09-08-00969-a.

References

1. N.A. Inogamov, V.V. Zhakhovskii, S.I. Ashitkov, V.A. Khokhlov, Yu.V. Petrov, P.S. Komarov, M.B. Agranat, S.I. Anisimov, K. Nishihara, Appl. Surf. Sci. **255**, 9712 (2009). arXiv: 0812.2965v1 [physics.optics]
2. W.-L. Chan, R.S. Averback, D.G. Cahill, A. Lagoutchev, Phys. Rev. B **78**, 214107 (2008)
3. S. Amoruso, R. Bruzzese, X. Wang, N.N. Nedialkov, P.A. Atanasov, J. Phys. D: Appl. Phys. **40**, 331 (2007)
4. N.A. Inogamov, Yu.V. Petrov, JETP **137**(2) (2010, in press)
5. Z. Lin, L.V. Zhigilei, V. Celli, Phys. Rev. B **77**, 075133 (2008)
6. V.V. Temnov, K. Sokolowski-Tinten, P. Zhou, D. von der Linde, J. Opt. Soc. Am. B **23**, 1954 (2006)

 Author's personal copy

7. V.V. Zhakhovskii, N.A. Inogamov Yu.V. Petrov, S.I. Ashitkov, K. Nishihara, Appl. Surf. Sci. **255**, 9592 (2009)
8. A.V. Bushman, G.I. Kanel', A.L. Ni, V.E. Fortov, *Intense Dynamic Loading of Condensed Matter* (Taylor & Francis, London, 1993), 295 p. http://teos.ficp.ac.ru/rusbank/
9. R. Courant, *Partial Differential Equations, vol. II* (Interscience, New York, 1962)
10. L.D. Landau, E.M. Lifshitz, *Fluid Dynamics*, 2nd edn., vol. 6 (Butterworth-Heineman, Oxford, 1987)
11. R. von Mises, *Mathematical Theory of Compressible Fluid Flow* (Academic Press, San Diego, 1958)
12. D.J. Funk, D.S. Moore, S.D. McGrane, K.T. Gahagan J.H. Reho, G.L. Fisher, S.D. McGrane, R.L. Rabie, Thin Solid Films **453–454**, 542 (2004)
13. L. Huang, Y. Yang, Y. Wang, Z. Zheng, W. Su, J. Phys. D: Appl. Phys. **42**, 045502 (2009)